

OPTICAL PROPERTIES AND DESIGN  
OF THE UNIVERSITY OF MANITOBA  
PROTON MICROPROBE

by

KOSAI ABDUL-RETHA

A THESIS

submitted to the Faculty of Graduate Studies  
in partial fulfilment of the requirements  
for the Degree of

MASTER OF SCIENCE

Department of Physics  
University of Manitoba  
WINNIPEG, Manitoba

1987 ©

Permission has been granted to the National Library of Canada to microfilm this thesis and to lend or sell copies of the film.

The author (copyright owner) has reserved other publication rights, and neither the thesis nor extensive extracts from it may be printed or otherwise reproduced without his/her written permission.

L'autorisation a été accordée à la Bibliothèque nationale du Canada de microfilmer cette thèse et de prêter ou de vendre des exemplaires du film.

L'auteur (titulaire du droit d'auteur) se réserve les autres droits de publication; ni la thèse ni de longs extraits de celle-ci ne doivent être imprimés ou autrement reproduits sans son autorisation écrite.

ISBN 0-315-37267-2

OPTICAL PROPERTIES AND DESIGN OF THE UNIVERSITY  
OF MANITOBA PROTON MICROPROBE

BY

KOSAI ABDUL-RETHA

A thesis submitted to the Faculty of Graduate Studies of  
the University of Manitoba in partial fulfillment of the requirements  
of the degree of

MASTER OF SCIENCE

© 1987

Permission has been granted to the LIBRARY OF THE UNIVER-  
SITY OF MANITOBA to lend or sell copies of this thesis. to  
the NATIONAL LIBRARY OF CANADA to microfilm this  
thesis and to lend or sell copies of the film, and UNIVERSITY  
MICROFILMS to publish an abstract of this thesis.

The author reserves other publication rights, and neither the  
thesis nor extensive extracts from it may be printed or other-  
wise reproduced without the author's written permission.

This thesis is dedicated to  
my great and loving parents  
and my wonderful wife.

*"Do for your present life  
as if you are living forever  
and  
Do for your later life  
as if you are dying tomorrow."  
(Imam Ali)*

## ABSTRACT

Since 1953 when the first device was built, the proton microprobe has become increasingly important as an analytical tool. This thesis describes work carried out to design the Manitoba Proton Microprobe. The Manitoba Microprobe is based on the "Russian quadruplet" lens system. The design goal was to achieve a minimum beam spot size using an iterative optimization procedure to arrive at a set of compromise values for several parameters. The optical characteristics of the "Russian quadruplet" lens configuration were investigated. A similar analysis was made on the pre-microprobe lens system; a magnetic doublet configuration. The microprobe system is optimized so that a spot diameter of 22.5  $\mu\text{m}$  is achieved for the range of proton energies provided by the cyclotron. A brief review of some existing proton microprobes is given with the description of the advantage of the Manitoba Proton Microprobe System.

## ACKNOWLEDGEMENTS

I would like to take this opportunity to express my sincere appreciation and thanks to the people who helped and supported me in this endeavour.

Thanks go to my supervisor, Professor J. S. C. McKee, Cyclotron Director, Physics Department, University of Manitoba, for his valuable advice during the course of this study, and for his constructive criticisms, suggestions and patience during the preparation of this manuscript.

I would also like to thank Dr. G. R. Smith, Physics Department, University of Manitoba, who has been an unfailing source of guidance from the very beginning of this work.

A special note of appreciation goes to Dr. K. Sharma and Dr. S. Oh of the Physics Department, University of Manitoba, for their provision of many valuable and helpful hints and also to Dr. M. S. A. L. Al-Ghazi for his moral support and encouragement.

Last, but not least, I would like to extend my utmost gratitude to my wife, Karen, for her helpfulness, encouragement and understanding during the course of this study.

## TABLE OF CONTENTS

	<u>PAGE</u>
DEDICATION	i
QUOTATION	ii
ABSTRACT	iii
ACKNOWLEDGEMENTS	iv
TABLE OF CONTENTS	v
LIST OF FIGURES	vii
LIST OF TABLES	xii
<u>INTRODUCTION</u>	1
<u>CHAPTER 1: ROLE AND FUNCTION OF THE PROTON MICROPROBE</u>	6
1.1 Historical review of the microprobe	7
1.2 Proton induced X-ray emission analysis with a microprobe	8
1.3 The function and variety of proton microprobes	11
1.3.1 Collimation microprobes	11
1.3.2 Focusing microprobes	13
<u>CHAPTER 2: REVIEW OF SOME OF THE EXISTING RELATED FACILITIES AND THE CHARACTERISTICS OF THE MANITOBA PROTON MICROPROBE</u>	17
2.1 Oxford Proton Microprobe	18
2.2 Heidelberg Proton Microprobe	19
2.3 Harwell Proton Microprobe	20
2.4 Zurich Proton Microprobe	22
2.5 Other conventional proton microprobes	23



	<u>PAGE</u>
2.6 Proton microprobes for cyclotron beams	25
2.7 The concept and the advantage of the Manitoba Proton Microprobe	27
<u>CHAPTER 3: THEORETICAL ASPECTS OF THE MANITOBA</u>	
<u>PROTON MICROPROBE</u>	29
3.1 First order matrix method	32
3.2 Matrix expansion to third order coordinates	42
<u>CHAPTER 4: DESIGN CONSIDERATIONS AND OPTIMIZATION</u>	
<u>OF BEAM OPTICS</u>	45
4.1 Beam optics analysis and lens performance	47
4.1.1 Analysis of the optical parameters of the microprobe lens	50
4.1.2 Optical characteristics of the pre-microprobe lens (magnetic doublet)	60
4.2 Higher order aberrations and fringing field effects	64
<u>CHAPTER 5: THE FINAL SYSTEM, CONSTRUCTION AND</u>	
<u>ASSEMBLY OF THE MICROPROBE FACILITY</u>	80
5.1 Arrangement of the final system	81
5.2 Construction and assembly of system elements	90
<u>CHAPTER 6: CONCLUSIONS AND FINAL REMARKS</u>	99
<u>REFERENCES</u>	104

## LIST OF FIGURES

<u>FIGURE</u>	<u>TITLE</u>	<u>PAGE</u>
1.1	Schematic diagram of the process of Proton Induced X-Ray Emission (PIXE) to produce the characteristic K and L x-rays.	10
1.2	Schematic diagram of the quadrupole magnet. a) the field orientations and components, and, b) the resultant force orientations, within the aperture.	15
4.1	The differential field variation inside the quadrupole magnet along the median plane.	48
4.2	The variation of the image dimensions and the required excitations with the separation distance between adjacent quadrupoles. $R_x$ and $R_y$ are half the dimension in x and y coordinates. Image distance, 0.03 m, object distance, 0.758 m and beam energy, 50 MeV for the quadruplet.  $B_1$ : the magnetic field setting of the outer two quadrupoles  $B_2$ : the magnetic field setting of the inner two	

<u>FIGURE</u>	<u>TITLE</u>	<u>PAGE</u>
	quadrupoles	52
4.3	The relationship between the normalized object distance (with respect to the effective length) and the image radius at image distance, 3 cm and separation distance, 8 cm for the quadruplet.	54
4.4	The variation of the image radius with the image distance at object distance, 1.458 m and separation distance, 8 cm for the quadruplet.	55
4.5	The variation of the image radius with the object distance at image distance, 10 cm and separation distance, 8 cm for the quadruplet.	58
4.6	Beam distribution and integral at the image plane (10 cm) at object distance, 1.808 m, separation distance, 8 cm, $\theta$ , 5.468 mrad., $\phi$ , 3.62 mrad, $\Delta E$ , 0.5% and standard fringing field (2000 particles).	72
4.7	Beam distribution and integral at the image plane (10 cm) at object distance, 1.808 m, separation distance, 8 cm, $\theta$ , 5.468 mrad, $\phi$ , 3.62 mrad, $\Delta E$ , 0.25% and standard fringing field (2000 particles).	73

<u>FIGURE</u>	<u>TITLE</u>	<u>PAGE</u>
4.8	Beam distribution and integral at the image plane (10 cm) at object distance, 1.808 m, separation distance, 8 cm, $\theta$ , 5.068 mrad, $\phi$ , 6.606 mrad, $\Delta E$ , 0.5% and standard fringing field (2000 particles).	75
4.9	Beam distribution and integral at the image plane (10 cm) at object distance, 1.808 m, separation distance, 8 cm, $\theta$ , 5.068 mrad, $\phi$ , 6.606 mrad, $\Delta E$ , 0.25% and standard fringing field (2000 particles).	76
4.10	Beam distribution and integral at the image plane (10 cm.) at object distance, 1.808 m, separation distance, 8 cm., $\theta$ , 2.232 mrad, $\phi$ , 2.5925 mrad., $\Delta E$ , 0.5% and standard fringing field (2000 particles).	77
4.11	Beam distribution and integral at the image plane (10 cm) at object distance, 1.808 m, separation distance, 8 cm, $\theta$ , 2.232 mrad, $\phi$ , 2.5925 mrad, $\Delta E$ , 0.25% and standard fringing field (2000 particles).	78

<u>FIGURE</u>	<u>TITLE</u>	<u>PAGE</u>
5.1	Map of the University of Manitoba Cyclotron and the experimental area. The arrow pointing at the proposed approximate position of the proton microprobe facility.	82
5.2	The beam envelope in the pre-microprobe magnetic doublet system. The object slit for the microprobe will be located at position S in this figure.	85
5.3	The beam envelope in the microprobe system from position S (object slit) to the image plane (target position).	87
5.4	The four slit configurations tested. The thickness of the slit material ( $t$ ) is identical for all the slits and is equal to the proton range (5.1 mm) at 50 MeV.	91
Plate 5.5	The collimator slit system which was built in the Faculty of Science Mechanical Workshop.	93
Plate 5.6	One of the two magnetic quadrupoles of the doublet system.	94

<u>FIGURE</u>	<u>TITLE</u>	<u>PAGE</u>
Plate 5.7	One of the microprobe quadrupole magnets before assembly. The figure shows the return path, a pole piece and one of the vacuum impregnated coils.	96
Plate 5.8	The specially designed high sensitivity adjustment cradle for the microprobe quadrupole magnets.	97

LIST OF TABLES

<u>TABLE</u>	<u>TITLE</u>	<u>PAGE</u>
4.1	Half-dimensions of the image in x and y coordinates and the magnetic fields (+ve: focus in x, defocus in y and -ve: defocus in x, focus in y) as a function of image distance at object distance, 1.458 m, lens separation distance, 8 cm and beam energy, 50 MeV (magnetic quadruplet) $B_1$ : the magnetic field setting of the outer two quadrupoles $B_2$ : the magnetic field setting of the inner two quadrupoles	56
4.2	Half-dimensions of the image in x and y coordinates and the magnetic fields (+ve: focus in x, defocus in y and -ve: defocus in x, focus in y) as a function of object distance at image distance, 10 cm, lens separation distance, 8 cm and beam energy, 50 MeV (magnetic quadruplet) $B_1$ : the magnetic field setting of the outer two quadrupoles $B_2$ : the magnetic field setting of the inner two quadrupoles	59

<u>TABLE</u>	<u>TITLE</u>	<u>PAGE</u>
4.3	<p>Half-dimensions of the image in x and y coordinates and the magnetic fields (+ve: focus in x, defocus in y and -ve: defocus in x, focus in y) as a function of beam energy at object distance, 1.808 m, image distance, 10 cm. and lens separation distance, 8 cm. (magnetic quadruplet)</p> <p><math>B_1</math>: the magnetic field setting of the outer two quadrupoles</p> <p><math>B_2</math>: the magnetic field setting of the inner two quadrupoles</p>	61
4.4	<p>Half-dimensions of the image in x and y coordinates and the magnetic fields of the doublet (+ve: focus in x, defocus in y and -ve: defocus in x, focus in y) as a function of magnet separation distance at object distance, 3.741 m, image distance, 1.247 m and beam energy, 50 MeV</p> <p><math>B_1</math>: the magnetic field setting of the first quadrupole in the beam direction</p> <p><math>B_2</math>: the magnetic field setting of the second quadrupole in the beam direction</p>	62



TABLETITLEPAGE

4.5	Half-dimensions of the image in x and y coordinates and the magnetic fields of the doublet (+ve: focus in x, defocus in y and -ve: defocus in x, focus in y) as a function of image distance at object distance, 2.841 m, magnet separation distance, 14 cm and beam energy, 50 MeV  $B_1$ : the magnetic field setting of the first quadrupole in the beam direction  $B_2$ : the magnetic field setting of the second quadrupole in the beam direction	63
4.6	Half-dimensions of the image in x and y coordinates and the magnetic fields of the doublet (+ve: focus in x, defocus in y and -ve: defocus in x, focus in y) at various selected conditions of object, image and separation distances at beam energy, 50 MeV  $B_1$ : the magnetic field setting of the first quadrupole in the beam direction  $B_2$ : the magnetic field setting of the second quadrupole in the beam direction  * The adopted combination for the final configuration.	65

4.7 The main aberration coefficients, half-dimensions of the image in x and y coordinates and the required magnetic fields for the quadruplet (+ve: focus in x, defocus in y and -ve: defocus in x, focus in y) as a function of the image distance at object distance, 1.358 m, separation distance, 8 cm, energy, 50 MeV and standard fringing field function.

$B_1$ : the magnetic field setting of the outer two quadrupoles

$B_2$ : the magnetic field setting of the inner two quadrupoles

66

4.8 The main aberration coefficient, half-dimensions of the image in x and y coordinates and the required magnetic fields for the quadruplet (+ve: focus in x, defocus in y and -ve: defocus in x, focus in y) as a function of the object distance at image distance, 10 cm, separation distance, 8 cm, energy, 50 MeV and standard fringing field function.

$B_1$ : the magnetic field setting of the outer two quadrupoles

$B_2$ : the magnetic field setting of the inner two

<u>TABLE</u>	<u>TITLE</u>	<u>PAGE</u>
	quadrupoles	67
4.9	The values of the main aberration coefficients in the quadruplet for various conditions. Object distance, 1.808 m, image distance, 10 cm, separation distance, 8 cm.	69
4.10	The half-dimensions of the image in the x and y and the magnetic fields of the quadruplet (+ve: focus in x, defocus in y and -ve: defocus in x, focus in y) as a function of object distance calculated at various conditions. Image distance, 10 cm, separation distance, 8 cm and beam energy, 50 MeV  B <sub>1</sub> : the magnetic field setting of the outer two quadrupoles  B <sub>2</sub> : the magnetic field setting of the inner two quadrupoles	71
5.1	The required magnetic field setting (+ve: focus in x, defocus in y and -ve: defocus in x, focus in y) as a function of beam energy. Object distance, 2.241 m, image distance, 2.147 m, separation distance, 20 cm (magnetic doublet).	

<u>TABLE</u>	<u>TITLE</u>	<u>PAGE</u>
	$B_1$ : the magnetic field setting of the first quadrupole in the beam direction	
	$B_2$ : the magnetic field setting of the second quadrupole in the beam direction	84
5.2	Half-dimensions and half-divergence angles of the proton beam in x and y coordinates at selected positions in the final microprobe system.	88

INTRODUCTION

## INTRODUCTION

A microprobe is a device which focuses a beam of ions into dimensions of a  $\mu\text{m}$  or less and is used for microanalysis in many fields of science. The electron microprobe, which focuses electrons, has developed into a precision instrument in recent years. Now, however, energetic ion microprobes are proving to have many advantages over the electron microprobe for analytical work. In particular, proton microprobes are beginning to play a major role in this field.

A proton microprobe is of value in many areas such as medicine, biology, metallurgy and geology. In the work presented in this text, a general, but qualitative description of the microprobe system is given. This comprises a summary of the beam optic theory involved in such systems and a survey of their configurations and overall performance. The University of Manitoba microprobe is based on the "Russian quadruplet" design of lens system (Dymnikov, 1965) which contains four magnetic quadrupole lenses.

In chapter (1), we explain the action of a microprobe facility in general and the rules governing its performances and characteristics. Various techniques for microbeam production are also reviewed. A comparison with the classical electron microprobe and the advantages of the proton microprobe over such systems are given in detail. A simple but adequate representation of a magnetic quadrupole and the field distribution inside the aperture is also presented. Chapter (2)

contains a historical review of proton microprobe development and its progress over the years. This is illustrated by a review of the major facilities which utilize beams with energies in the range from 1-6 Mev from tandem and single-ended Van de Graaff accelerators as well as facilities which use beams extracted from higher energy cyclotrons. Through this review, the capability of different lens configurations and arrangements in producing the microprobe image is identified through a review of available and reported data. At the end of this chapter, we give the characteristics of our adopted design and the many advantages this system may offer.

The theoretical aspects of such devices are of importance. The matrix method is one of the most common techniques applied by scientists to beam transport system analysis today. We have employed in our study two computer codes which utilize this particular method for beam optic calculations. The method is described and derived from the equations of motion of the beam in chapter (3). The derivation is initially made by using a transfer matrix representation to first order for each system element. Matrix multiplication is carried out in that fashion for the "Russian quadruplet" lens configuration which has been chosen for our microprobe facility. The main lens parameters are then derived from the elements of the final matrix. The method for expanding the transfer matrix from the first order to include coefficients of up to and including the third order is then presented in a simple form.

In order to understand the relationships between the many lens and beam parameters and the influence of such relationships on the microbeam spot size we have attempted to assess the effects of varying one parameter or more at a time and record the change in other factors in chapter (4). The effects of the separation distance between neighboring quadrupoles, object distance, image distance, beam energy and divergence angles, etc., on the spot size are examined. Calculations involving aberration coefficients to third order are essential in any lens system analysis since the contribution of such aberrations is very large and destructive to the image quality and size. The effects of the main aberration coefficients on the lens and the beam parameters were determined under various assumptions such as: a) fringing field effects are ignored and b) two particular kinds of fringing field functions are considered. Graphic figures of the distribution of protons at the image plane considering up to third order effects were obtained from a Monte Carlo simulation technique. These figures have displayed the contributions of the chromatic and the spherical aberrations to the spot size for different values of energy spread and beam divergence angles.

From the results of the analysis and calculations of chapter (4), optimization processes were followed for the purpose of realizing the best configuration for our design. The calculations also provided the acceptable initial beam parameters for the microprobe system so that an optimum image size could be obtained. The final design of our microprobe facility is reported in chapter (5). Further, details about



the tests performed on the lens elements, the construction procedure for these elements and the final assembly of the system are given.

In the last chapter, we reach a number of conclusions and make suggestions which result from this study.

CHAPTER 1

ROLE AND FUNCTION OF THE PROTON MICROPROBE

## CHAPTER 1

### ROLE AND FUNCTION OF THE PROTON MICROPROBE

#### 1.1 Historical review of the microprobe

Electron microprobes have been in existence for the last fifty years and are used for x-ray analysis in various branches of science. It was not until the end of the 1960's that physicists started to think of possible ways to reduce the large background effects associated with an electron microprobe. By combining the enormous knowledge of electron optics and the accelerator related ion optics<sup>1</sup>, scientists made the first step towards the development of a new and more sophisticated analytical tool, the proton microprobe.

Using proton microbeams rather than electron microbeams has many advantages. The total bremsstrahlung background observed in electron systems is reduced in the proton microprobe since it is proportional to the square of  $m_e/m_p$ <sup>2,3</sup>. The proton microprobe allows us to detect certain undetectable trace elements (e.g. rare earth) at the ppm level<sup>4</sup> which cannot be detected by the electron microprobe. This fact has been demonstrated on various occasions. An additional advantage of proton microbeams is their low multiple scattering of protons compared to electron microbeams. This is due to their higher energy<sup>1</sup> and mass. Our system will utilize a new analytical technique of beam transmission

through a very thin target to produce a monoenergetic x-ray emission.

The first ion microbeam ever produced was in 1953 by Zirkle and Bloom<sup>5</sup> using the collimation method. However, Cookson et al. had the privilege of building the first focusing proton microprobe at A.E.R.E., Harwell in 1969<sup>5</sup>. Since then the number of existing microprobes has grown exponentially. Most of these systems focus the proton beam to a few micrometers in spot size and such resolutions are sufficient for most applications of the instrument. However, an interest in examining samples of dimensions down to a micron in size has established the need for smaller beam sizes; a fact which has encouraged system designers to search for methods of reducing the contribution of aberrations to beam spot size. Recently, Microscope Associates, Inc. have reported their achievement in producing a  $0.5 \times 0.5 \mu\text{m}^2$  spot at 1.2 MeV proton energy from an achromatic magnetic doublet<sup>6</sup>.

## 1.2 Proton induced x-ray emission analysis with a microprobe

It has been reported<sup>7</sup> that proton induced x-ray emission (PIXE) was first used as an analytical technique for trace elements in 1968. Since that time the tool has been widely accepted as a powerful analytical method for detecting multiple elements simultaneously with high sensitivity in many instances to ppb. This high sensitivity has been reached because of the development of high resolution x-ray detectors. Another advantage of using PIXE for trace element analysis is its characteristic of being non-destructive to the analyzed sample.

PIXE is produced by an atomic process in which there is an energy dependent probability that a proton at high energy will knock out an inner-shell electron from atoms in the target. When electrons from higher energy levels move to fill the gap created by the ejected electron, an x-ray quantum will be emitted (figure 1.1). The energy of this emitted x-ray is characteristic of the target atom. By using high resolution solid-state detectors, which can detect a wide range of x-rays as well as resolving various energies of x-rays efficiently, we can obtain information about the elements and their concentrations in the target under consideration.

There are however some difficulties inherent with the PIXE method. The detection limits are determined by x-ray production cross sections and the continuous background radiation which results from the interaction of the proton beam with the sample<sup>8</sup>. Since the K x-ray production cross-section is a function of incident particle energy, the study of such rays should be constructed at that proton energy for which the yield is maximum<sup>9</sup>.

With PIXE, samples are irradiated with proton beams of size 2 mm in diameter and results obtained for relatively large areas of the sample. These results are accurate enough to give the elemental composition of a sample with no reference to the elemental distribution within the sample. The concept of the microprobe is to reduce the beam size to the  $\mu\text{m}$  level so that it becomes smaller than the size of a plant or animal tissue cell. Once this is achieved, we will have a more

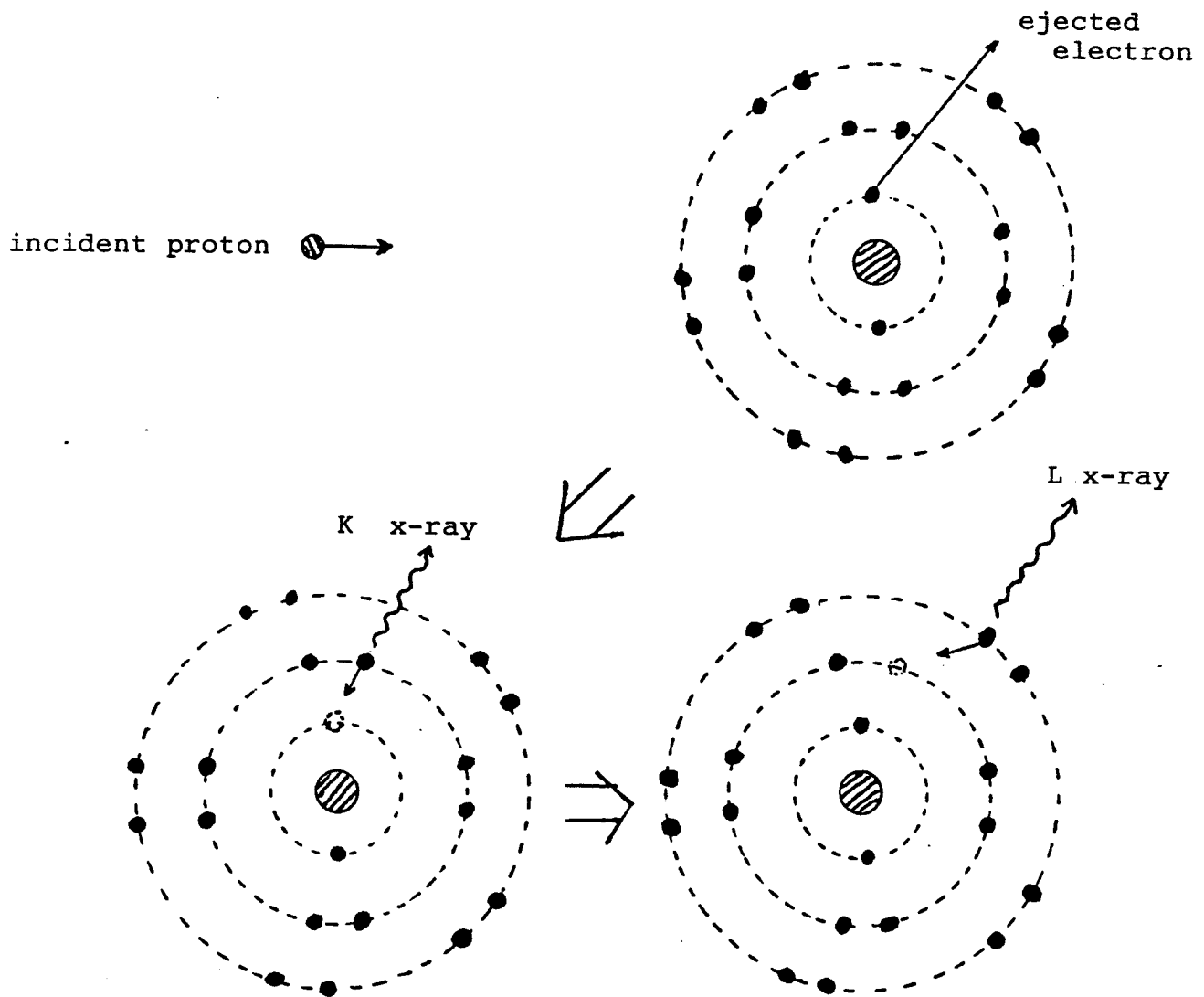


Figure 1.1 Schematic diagram of the process of Proton Induced X-Ray Emission (PIXE) to produce the characteristic K and L x-rays.

powerful tool for analysis.

Information may be obtained by scanning the beam in order to survey the chemical composition of the cell itself. This valuable, detailed information on trace elements, which includes their concentration and distribution within microscopic volumes of the sample, is of great importance in advancing several areas of science.

### 1.3 The function and variety of proton microprobes

As described above, the objective of building a proton microprobe is to find a means to focus a proton beam to a few micrometers or even a fraction of a micrometer in size. Two available techniques can be employed to achieve such a small beam dimension; collimation or focusing the particle beams.

#### 1.3.1 Collimation microprobes

This is the simplest of the two techniques. It does not employ any type of lens to produce fine beams. The beam dimensions are defined by a collimating diaphragm and depend upon the degree of beam scattering from the collimating edge. As previously mentioned, the first microbeam was produced using this method seventeen years before the first focusing microprobe was built at Harwell. This microbeam was satisfactory for the purpose at the time, which was to study the effect of radiation on animal cells. There are several drawbacks which set limitations on the

use of a collimated microbeam. The transmitted current of the collimated beam is proportional to the area of the collimating aperture. The scattering of particles from the slit edge adds a halo to the beam size which is proportional to the circumference of the slit<sup>5</sup>. Separate studies have been done to improve the performance of the slit by studying the effect of slit thickness and shape on the beam scattering. This topic will be discussed in chapter (5). Since the collimation microprobe employs no focusing elements, the angular divergence of the beam after passing through the collimating slit should be very small so as to minimize the beam spreading when it hits the target<sup>10</sup>. This can be made possible by using a lens system prior to the collimator; however, Liouville's theorem, which states that the emittance of a beam with fixed energy is a constant, implies that any reduction in the divergence of the beam at the object position will result in an increase in its dimensions at the image position and therefore creates a large reduction in the beam intensity after passing through the collimator.

To avoid low beam intensity while simultaneously maintaining a narrow beam, the target has to be placed very close to the collimation system. Again this presents another problem, namely that of higher background radiation from the collimator material. It has also been found that practically, it is difficult to construct a microcollimator with a diameter less than 10  $\mu\text{m}$  from material thick enough to stop the incoming beam<sup>10</sup>.



### 1.3.2 Focusing microprobes

This method is far superior to the above technique and has been employed by most laboratories around the globe. Most of the problems associated with the collimating technique may be overcome by this method. Basically, it requires a focusing system to receive the beam emerging from an object slit and demagnify it to a few  $\mu\text{m}$ 's or smaller. This focusing system may be designed to focus in one or two steps. There are several problems which arise from using a two-step focusing system. Because of the very long two-step system, it is very difficult to achieve stability and precision for such small beam sizes. Moreover, the residual gas scattering will increase the beam emittance and the aberrations are higher than in single-step focusing<sup>8</sup>.

The focusing system may be constructed using electrostatic or magnetostatic lenses. Electrostatic lenses can be used successfully with low energy beams in the KeV range, however, with beams of higher energies in the MeV range (the lowest range used for proton microprobe analysis) it becomes difficult to employ such a lens system. Solenoids are commonly used in most electron microprobes today, as is the case with low energy ion probes. There are, however, practical and economic limitations to the use of such lenses for high energy proton microprobes. The other alternative is to consider the strong focusing quadrupole magnet. This type of magnet can provide the desired focusing with fields of moderate strength. The majority of the focused proton

microprobe laboratories use quadrupole lenses.

The principle of focusing by a quadrupole magnet is well documented and studies have continued for many decades to improve the pole tip shape resulting in a more homogeneous magnetic field distribution containing fewer field harmonics. Quadrupole magnets have four identical poles, alternately N and S, as shown schematically in figure 1.2.

As can be seen from the orientations in figure 1.2, the final effect of the magnet is focusing in the xz-plane and defocusing in the yz-plane. The field is zero at the centre of the aperture and increases linearly as we move away from the centre in a particular direction. Typically, this field variation should provide a constant field gradient. However, this may not be the case everywhere within the aperture due to the effects of pole shape on the field distribution. Since a quadrupole magnet focuses in one plane and defocuses in the other, two such magnets are required to obtain focusing of the beam in both planes.

Magnetic quadrupole multiplets are not the only type of lens employed for probe-forming systems. At Los Alamos<sup>11</sup>, they are using a superconducting solenoid to obtain beam sizes of 5  $\mu\text{m}$  in diameter. The only limitation imposed on this lens is due to the chromatic aberrations. Although this type of superconducting solenoidal lens

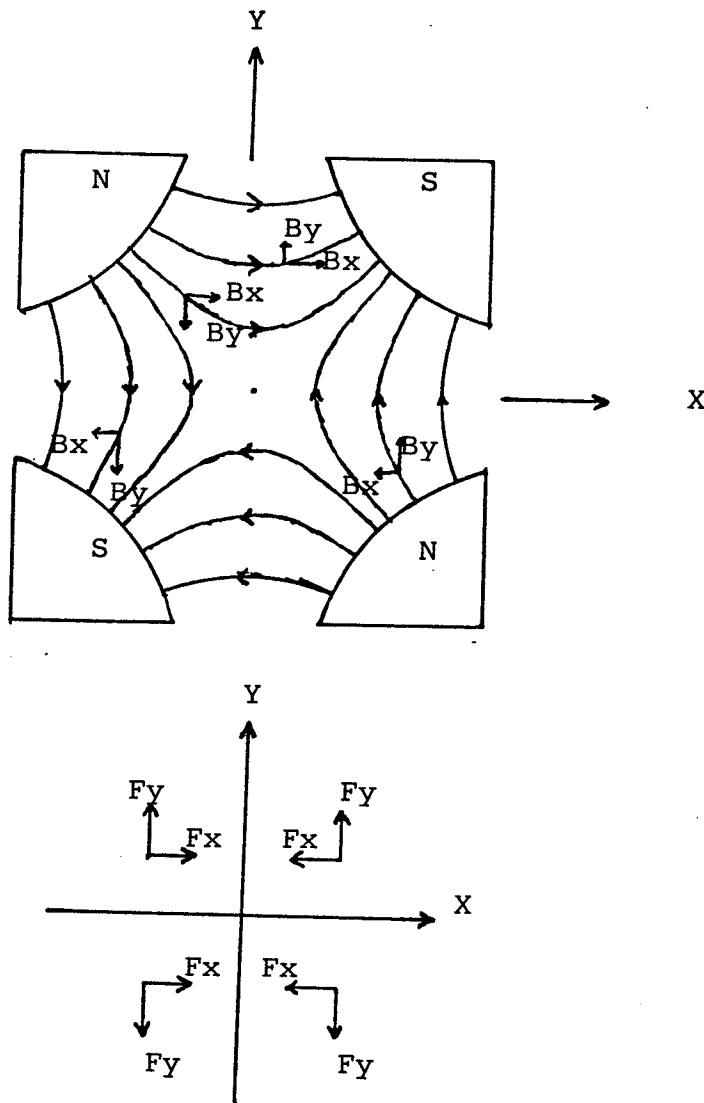


Figure 1.2

Schematic diagram of the quadrupole magnet.  
 a) the field orientations and components,  
 and,  
 b) the resultant force orientations, within  
 the aperture.

represents a very interesting development in this field, it still cannot be taken as a replacement for the magnetic quadrupole multiplet.

CHAPTER 2

REVIEW OF SOME OF THE EXISTING RELATED  
FACILITIES AND THE CHARACTERISTICS OF  
THE MANITOBA PROTON MICROPROBE

## CHAPTER 2

### REVIEW OF SOME OF THE EXISTING RELATED FACILITIES AND THE CHARACTERISTICS OF THE MANITOBA PROTON MICROPROBE

According to Legge<sup>13</sup> 1982, there are about 27 focused proton microprobe systems currently in use. A majority of these facilities focus beams by means of combinations of quadrupole magnets. The various possible combinations will be described when we review some of the reported facilities. In addition to the focused proton microprobes, there are several collimation proton microprobe systems in operation<sup>12</sup>. Our interest is in focusing proton microprobes. Only references pertaining to the collimation type will be given here. At Birmingham University, a beam from a 3 MeV dynamitron is collimated to 20-1000  $\mu\text{m}$  in diameter and is mainly used for material science. A 2 MeV beam from a Van de Graaff accelerator is collimated to 50-500  $\mu\text{m}$  at Delaware University, Bartol. At Brooklyn College, N.Y. and Queen's University, Kingston, beams from 4 MeV Van de Graaff accelerators are successfully collimated to 20  $\mu\text{m}$  and 10  $\mu\text{m}$  respectively. There are several other collimation proton microprobes which have been reported<sup>5</sup> which may or may not still be on-line today.

#### 2.1 Oxford Proton Microprobe

In this system, which has been operational since 1978<sup>5</sup>, they have

adopted the coupled triplet CDC\* where the first and the second quadrupole lenses are coupled together to have the same excitation. Although this configuration suffers from relatively high intrinsic and parasitic aberration coefficients<sup>4</sup>, the xz- and yz- demagnifications of 66 and 15 respectively, provide a  $1 \times 1 \mu\text{m}^2$  spot size with an  $80 \text{ pA}/\mu\text{m}^2$  current density<sup>10</sup>. An adjustable stainless steel object aperture is located 5.786 m from the first quadrupole. Due to this relatively long object distance, collimator slits are used to control the beam envelope in order to match the lens aperture. The quadrupole magnets are composed of Swedish iron<sup>12</sup> and are individually adjustable in all directions. Each quadrupole has an effective length of 21.4 cm and has an aperture with a radius of 1.5 cm. The space between the adjacent quadrupoles is 4.6 cm and the image distance is 16 cm for the above given spot size<sup>4</sup>. This facility is used to focus a proton beam from a 4 MeV EN tandem Van de Graaff accelerator.

## 2.2 Heidelberg Proton Microprobe

This facility was built in 1976<sup>5</sup> and may be one of the shortest systems (2.1 m) capable of focusing a proton beam from a 6 MeV EN tandem Van de Graaff accelerator to approximately a  $2 \times 2 \mu\text{m}^2$  spot size<sup>13</sup> and a current density of  $20 \text{ pA}/\mu\text{m}^2$ . This is achieved by a short, but

---

\* The symbols of the combinations in this text are used to refer to the lens action in the xz-plane. The letters C and D indicate the converging and diverging elements respectively. Clearly it implies the opposite action in the yz-plane.

powerful, high gradient (400 T/m), magnetic quadrupole doublet of CD configuration<sup>14</sup>. The high magnetic field gradient was obtained by choosing a very narrow quadrupole aperture, 2.5 mm in radius<sup>8</sup>, in addition to positioning the wound coil very close (4 mm) to the aperture. The achieved xz- and yz-demagnifications are 4 and 23 respectively at approximately a 10 cm image distance. The aberrations are low. Moreover, for the magnet material, the choice of 50% Fe and 50% Co alloy with a saturation of 2.3 T, together with the material's special treatment were essential for obtaining the good performance. The system employed two sets of collimator slits<sup>15</sup>. They are of an ingenious design due to Nobiling and are used to adjust the area as well as the divergence of the beam. The first collimator set, which is used to define the object slit, has the front edges made of tungsten carbide. Such material allows for very smooth surfaces and can be attained with approximately a 0.05  $\mu\text{m}$  roughness<sup>8</sup> which has the effect of greatly reducing the slit scattering. The second collimator set is located one meter downstream from the first one to independently adjust the beam divergences in the xz- and yz-planes to define the acceptance of the lens. The effective length of each quadrupole singlet is approximately 4.27 cm and the separation distance within the doublet is 4 cm.

### 2.3 Harwell Proton Microprobe

As has been reported earlier, this is the oldest (1969) high energy focusing proton microprobe ever built. The "Russian quadruplet" of antisymmetric CDCD configuration is utilized for beam focusing to